Paper 8

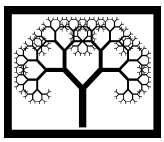

Proceedings of the Seventh International Conference
on Computational Structures Technology,
B.H.V. Topping and C.A. Mota Soares (Editors),
Civil-Comp Press, Stirling, Scotland.

Classical and Optimal Active Vibration Control of Smart Piezoelectric Beams

C.M.A. Vasques and J.D. Rodrigues
Department of Mechanical Engineering and Industrial Management
Faculty of Engineering, University of Porto, Portugal

Abstract

In this paper a numerical study concerning the active vibration control of smart piezoelectric beams is presented. A comparison between the classical control strategies, constant gain and amplitude velocity feedback, and optimal control strategies, linear quadratic regulator (LQR) and linear quadratic Gaussian (LQG) controller, is performed in order to investigate their effectiveness to suppress vibrations in beams with piezoelectric patches with sensing and actuating capabilities.

As a mathematical model, a one-dimensional finite element of a three-layered smart beam with two piezoelectric surface layers and metallic core is utilized and briefly presented. The mathematical model considers a partial layerwise theory, with three discrete-layers, and a fully coupled electro-mechanical theory. The finite element model equations of motion and electric charge equilibrium are presented and recast into a state variable representation in terms of the physical modes of the beam.

The analyzed case studies concern the vibration reduction of a cantilever aluminum beam with a pair of collocated piezoelectric patches mounted on the surface. The displacement time history, for an initial displacement field and white noise force disturbance, and point receptance at the free end are evaluated with the open- and closed-loop classical and optimal control systems. The case studies allow to compare their performances and demonstrate their advantages and disadvantages.

Keywords: smart piezoelectric beam, finite element, active vibration control, velocity feedback, LQR and LQG controller.

1 Introduction

The objective of active vibration control is to reduce the vibration of a mechanical system by the automatic modification of the system's structural response. An active structure consists of a structure provided with a set of sensors (to detect the vibra-

tion) and actuators (which influence the structural response of the system) coupled by a controller (to suitably manipulate the signal from the sensor and change the system's response in the required manner). Structures which have the distinctive feature of having sensors and actuators that are often distributed and have a high degree of integration inside the structure are called *smart* structures.

Some of the most widely used distributed sensors and actuators are made of piezoelectric materials. The piezoelectric effect consists of the ability of certain crystalline materials to generate an electrical charge in proportion of an externally applied force (*direct* piezoelectric effect) and to induce an expansion on the piezoelectric material in proportion to an electric field parallel to the direction of polarization (*inverse* piezoelectric effect). There are two broad classes of piezoelectric materials used in vibration control: polymers and ceramics. The piezopolymers are used mostly as sensors because they require extremely high voltages and the piezoceramics are extensively used as actuators and sensors for a wide range of frequency.

Modelling smart structures often requires a coupled modelling between the structure and the piezoelectric sensors and actuators. They can be modeled as either lumped or distributed parameter systems, and usually these systems have complicated shapes and structural patterns that make the development and solution of descriptive partial differential equations burdensome, if not impossible. Alternatively, various discretization techniques, such as finite element (FE) modelling, modal analysis, and lumped parameters, allow the approximation of the partial differential equations by a finite set of ordinary differential equations. Since the 70's, many FE models have been proposed for the analysis of smart piezoelectric structural systems. A survey on the advances in piezoelectric FE modelling of adaptive structural elements is presented by Benjeddou [1]. On the development of FE models, different assumptions can be taken into account in the theoretical model when considering the electro-mechanical coupling. These assumptions regard mainly the use (or not) of electric degrees of freedom (DoF) and the approximations of the through-the-thickness variation of the electric potential. Therefore, they lead to decoupled, partial and fully coupled electro-mechanical theories, which in turn can lead to different modifications of the structure's stiffness and different approximations of the physics of the system. These electro-mechanical coupling theories can be considered by the use of *effective stiffness parameters*, defined according the electric boundary condition considered, as shown by Vasques and Rodrigues [2] for a smart beam.

Several methods have been applied to the active vibration control in the engineering field. The recent advances in digital signal processing and sensors and actuators technology have prompted interest in active vibration control [3–6]. In the past two decades, various methods of active vibration control have been developed. A review about the active structural vibration control is presented in reference [7]. The different algorithms utilized in active vibration control can be classified under two general categories: *feedforward* and *feedback* control. Variations of the two general methods exist, each with advantages, disadvantages, and limitations.

This work is entirely devoted to feedback control where we are particularly con-

cerned with systems in which the excitation of the structure can not be directly observed and thus cannot be used as a feedforward control signal. The control systems discussed in this work will be those in which the control signal obtained from the piezoelectric sensor, which is affected by both the excitation force (primary excitation) and the piezoelectric actuator voltage (secondary excitation, over which we have control), is *fed back* to the actuator.

As noted by Preumont [6], one of the objectives of control can be to reduce the resonant peaks of the frequency response function, which is known as *active damping*. It can be achieved without a model of the structure and with guaranteed stability, provided that the actuator and sensor are collocated and have perfect dynamics. Another objective of the control can be to reduce the effects of external disturbances in order to keep a control variable (e.g. a position) to a desired value in some frequency range, which is known as *model based* feedback. The design problem consists of finding the appropriate compensator such that the closed-loop system is stable and behaves in an appropriate manner. These model based strategies are global methods which manage to attenuate all the disturbances in the frequency range of analysis. In compensation they require a mathematical model of the system (e.g. FE model), have a bandwidth limited by the accuracy of the model and may amplify the disturbances outside the bandwidth (*spillover*).

The aims of this work are the analysis and comparison of the classical and optimal feedback control strategies on the active control of vibrations of smart piezoelectric beams. In this paper we start by succinctly describe the mathematical model utilized and a brief description of the one-dimensional FE developed by Vasques and Rodrigues [2] is presented. The kinematic and electric potential assumptions of the theoretical and FE spatial model are first presented. Next, the resultant FE equations of motion and electric charge equilibrium are presented and recast into a state variable representation in terms of the physical modes of the beam. Moreover, some theoretical considerations about the classical control strategies, with two distinct velocity feedback control algorithms being utilized, *constant amplitude* and *constant gain* velocity feedback (CAVF and CGVF), and optimal control strategies, *linear quadratic regulator* (LQR) and *linear quadratic Gaussian* (LQG) controller, are presented. The control models assume that one of the piezoelectric layers acts as a distributed sensor and the other one as a distributed actuator, and the sensor signal is used as a feedback reference in the closed-loop control systems.

Finally, a case study concerning the vibration of a cantilever aluminium beam with a pair of collocated piezoelectric patches mounted on the surface is analyzed. The displacement time history, for an initial displacement field and white noise force disturbance, and point receptance at the free end are evaluated with the open- and closed-loop classical and optimal control systems.

2 Mathematical Model

2.1 Kinematic and Electrical Assumptions

Consider the three-layered beam illustrated in Figure 1. The axial and transverse displacements, $u_k(x,z,t)$ and $w_k(x,z,t)$, of the metallic core (c) and two piezoelectric surface layers (a,b) are defined by

$$u_c(x,z,t) = u_0(x,t) + z_c\theta_c(x,t), \tag{1a}$$

$$u_a(x,z,t) = u_0(x,t) - \frac{h_c}{2}\theta_c(x,t) + \left(z_a - \frac{h_a}{2}\right)\theta_a(x,t), \tag{1b}$$

$$u_b(x,z,t) = u_0(x,t) + \frac{h_c}{2}\theta_c(x,t) + \left(z_b + \frac{h_b}{2}\right)\theta_b(x,t), \tag{1c}$$

$$w_k(x,z,t) = w_0(x,t), \tag{2}$$

where the subscript $k = a,b,c$ is the layer reference, h_k is the thickness of each layer, $u_0(x,t)$ and $w_0(x,t)$ are the axial and transverse displacements of the beam's mid-plane, and $\theta_k(x,t)$ is the rotation of each layer. Note that axial displacement continuity at the interfaces of the layers is assured, leading to coupling terms in the axial displacement $u_k(x,z,t)$ of the layers, and that constant through-the-thickness transverse displacement $w_0(x,t)$ is considered. According to the displacement definitions in Equations (1) and (2), the extensional and shear mechanical strains of the layers can be determined by the usual linear strain-displacement relations, where the kinematic assumptions lead to null transverse strains and a first-order shear deformation theory for the three layers (see [2] for further details).

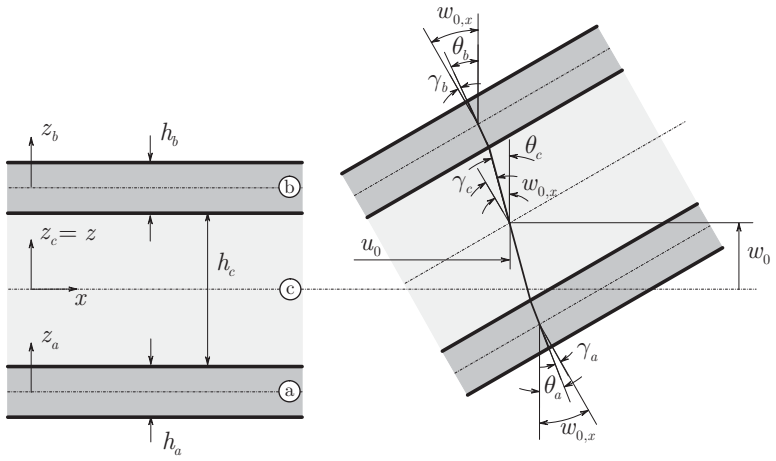

Figure 1: Three-layered beam displacement field.

The piezoelectric materials considered for the surface layers are orthotropic with the directions of orthotropy coincident with the axes of the beam. Those materials are

polarized in the transverse direction and have the behavior of the standard piezoelectric materials [10, 11]. The electrical model takes the direct piezoelectric effect into account and a quadratic trough-the-thickness distribution of the electric potential and an appropriate approximation of the x-component of the electric field are considered (see [2] for further details).

2.2 Spatial Model

The FE spatial model is obtained from the weak integral forms of the equations of motion and electric charge equilibrium presented in reference [2]. They are derived using Hamilton's principle where the Lagrangian and the applied forces total work are conveniently adapted for the electrical and mechanical contributions. The one-dimensional smart beam FE considers a fully coupled electromechanical theory and has two nodes, with five mechanical degrees of freedom (DoF) per node (the axial and transverse displacements of the beam's mid-plane and the rotation of each layer), and two electric DoF per element (the electric potential difference of each piezoelectric layer). The FE assumes Lagrange linear shape functions for the mechanical DoF and the electrical DoF are assumed constant and uniform in the element. Therefore, the elementary mechanical and electrical DoF vectors, $\bar{\mathbf{u}}^e(t)$ and $\bar{\boldsymbol{\phi}}^e(t)$, are as follows:

$$\bar{\mathbf{u}}^e(t) = \{\bar{u}_0^1, \bar{w}_0^1, \bar{\theta}_a^1, \bar{\theta}_c^1, \bar{\theta}_b^1, \bar{u}_0^2, \bar{w}_0^2, \bar{\theta}_a^2, \bar{\theta}_c^2, \bar{\theta}_b^2\}^{\mathrm{T}}, \;\; \bar{\boldsymbol{\phi}}^e(t) = \{\bar{\phi}_a, \bar{\phi}_b\}^{\mathrm{T}}. \tag{3a,b}$$

The resultant global FE spatial model, governing the motion and electric charge equilibrium, is given by

$$\mathbf{M}_{uu}\ddot{\bar{\mathbf{u}}}(t) + \mathbf{K}_{uu}\bar{\mathbf{u}}(t) + \mathbf{K}_{u\phi}\bar{\boldsymbol{\phi}}(t) = \mathbf{F}(t), \tag{4}$$

$$\mathbf{K}_{\phi u}\bar{\mathbf{u}}(t) + \mathbf{K}_{\phi\phi}\bar{\boldsymbol{\phi}}(t) = \mathbf{Q}(t), \tag{5}$$

where $\bar{\mathbf{u}}(t)$ and $\bar{\boldsymbol{\phi}}(t)$ are the global mechanical and electrical DoF vectors, $\mathbf{M}_{uu}$ and $\mathbf{K}_{uu}$ are the global mass and stiffness matrices, $\mathbf{K}_{u\phi} = \mathbf{K}_{u\phi}^{\mathrm{T}}$ is the global piezoelectric stiffness matrix, $\mathbf{K}_{\phi\phi}$ is the global capacitance matrix and $\mathbf{F}(t)$ and $\mathbf{Q}(t)$ are the global mechanical force and electric charge vectors.

The electrical DoF vector in Equations (4) and (5) can be divided in the actuating and sensing DoF, $\bar{\boldsymbol{\phi}}(t) = \{\bar{\boldsymbol{\phi}}_{\mathrm{a}}(t), \bar{\boldsymbol{\phi}}_{\mathrm{s}}(t)\}^{\mathrm{T}}$, where the subscripts 'a' and 's' denote the actuating and sensing capabilities. Hence, considering open-circuit electrodes, and in that case $\mathbf{Q}(t) = 0$, the non specified potential differences in (5) can be statically condensed in (4) and the equations of motion and charge equilibrium become

$$\mathbf{M}_{uu}\ddot{\bar{\mathbf{u}}}(t) + \mathbf{K}_{uu}^{*}\bar{\mathbf{u}}(t) = -\mathbf{K}_{u\phi\mathrm{a}}\bar{\boldsymbol{\phi}}_{\mathrm{a}}(t) + \mathbf{F}(t), \tag{6}$$

$$\bar{\boldsymbol{\phi}}_{\mathrm{s}}(t) = -\mathbf{K}_{\phi\phi\mathrm{s}}^{-1}\mathbf{K}_{\phi u\mathrm{s}}\bar{\mathbf{u}}(t), \tag{7}$$

with

$$\mathbf{K}_{uu}^{*} = \mathbf{K}_{uu} - \mathbf{K}_{u\phi\mathrm{s}}\mathbf{K}_{\phi\phi\mathrm{s}}^{-1}\mathbf{K}_{\phi u\mathrm{s}}. \tag{8}$$

It's worth to note that a non-null parabolic through-the-thickness distribution of the electric potential within the piezoelectric layers was already considered in the variational formulation through the use of effective stiffness parameters (see [2]). Moreover, the static consensation in Equation (8) only considers the linear term of the electrical potential distribution, which is the one that in fact contributes to the sensor voltage.

2.3 Modal Model

In the process of designing an active control system one can utilize a full model of the system and, consequently, a higher computational effort is needed, or a reduced model of the system, which requires a lower computational effort. However, the structural mathematical model and controller design are not independent aspects of vibration control. Flexible structures are distributed parameter systems that have an infinite number of DoF, and a feedback controller based on a reduced modal model can destabilize the residual modes (unmodeled dynamics) leading to observation and control spillover problems. They both degrade the system's performance, and the former can even cause the system to become unstable [4]. Methods to reduce the effects of spillover are discussed by Balas [9].

When excited a structure presents preferable modes of vibration which depend of the spectral content of the excitation. Assuming that the lower order modes, which have lower energy associated and consequently are the more easily excitable ones, are the more significant to the global response of the system, a truncated modal matrix $\hat{\mathbf{\Psi}}$ can be utilized as a transformation matrix between the generalized coordinates $\bar{\mathbf{u}}(t)$ and the modal coordinates $\boldsymbol{\eta}(t)$. Thus, the displacement vector $\bar{\mathbf{u}}(t)$ can be approximated by the modal superposition of the first r modes,

$$\bar{\mathbf{u}}(t) = \sum_{i=1}^{r} \mathbf{\Psi}_i \eta_i(t) = \hat{\mathbf{\Psi}} \boldsymbol{\eta}(t), \tag{9}$$

where $\hat{\mathbf{\Psi}} = [\mathbf{\Psi}_1, \cdots, \mathbf{\Psi}_r]$ is the truncated modal matrix and $\boldsymbol{\eta}(t) = \{\eta_1(t), \cdots, \eta_r(t)\}^{\mathrm{T}}$ the correspondent modal coordinates vector. Hence, the system's size isn't anymore the total number of DoF of the FE model but the number of modes chosen to model it.

The spatial stiffness and mass matrices obtained with the FE method typically present a band structure, which represents the coupling between the several DoF, that makes the spatial damping matrix difficult to be obtained. In this study a proportional viscous damping model is utilized and the spatial damping matrix $\mathbf{D}_{uu}$, according to the orthogonality properties of the modal vectors with respect to the mass and stiffness matrices, is diagonalized by the truncated modal matrix $\hat{\mathbf{\Psi}}$,

$$\hat{\mathbf{\Psi}}^{\mathrm{T}} \mathbf{D}_{uu} \hat{\mathbf{\Psi}} = \mathbf{\Lambda}, \tag{10}$$

and a diagonal modal damping matrix $\mathbf{\Lambda}$ with the generic term $2\xi_i\omega_i$, where ξ_i is the modal damping ratio and ω_i the undamped natural frequency of the i-th mode, is obtained. Hence, that considerably simplifies the inclusion oh the inherent damping

effects in our model. Considering a normalization scheme for unitary modal masses, Equations (6) and (7) with the modal damping matrix included become

$$\ddot{\boldsymbol{\eta}}(t) + \boldsymbol{\Lambda}\dot{\boldsymbol{\eta}}(t) + \boldsymbol{\Omega}\boldsymbol{\eta}(t) = -\hat{\boldsymbol{\Psi}}^{\mathrm{T}}\mathbf{K}_{u\phi\mathrm{a}}\bar{\boldsymbol{\phi}}_{\mathrm{a}}(t) + \hat{\boldsymbol{\Psi}}^{\mathrm{T}}\mathbf{F}(t), \tag{11}$$

$$\bar{\boldsymbol{\phi}}_{\mathrm{s}}(t) = -\mathbf{K}_{\phi\phi\mathrm{s}}^{-1}\mathbf{K}_{\phi u\mathrm{s}}\hat{\boldsymbol{\Psi}}\boldsymbol{\eta}(t), \tag{12}$$

where $\boldsymbol{\Omega}$ is a diagonal matrix with the generic term ω_i^2. Equations (11) and (12) represent the truncated modal model of the smart piezoelectric beam.

3 Active Control of Vibrations

3.1 State Space Design

The state space approach is the basis of the modern control theories and is strongly recommended in the design and analysis of control systems with a great amount of inputs and outputs [8]. In this method, dynamic systems are described by a set of first-order differential equations in variables called the *state*.

According to Equations (11) and (12) the state variables are chosen as follows,

$$\mathbf{x}(t) = \left\{ \begin{array}{c} \boldsymbol{\eta}(t) \\ \dot{\boldsymbol{\eta}}(t) \end{array} \right\}, \tag{13}$$

and the open-loop system is represented by two first-order matricial differential equations expressed in terms of the state variables vector $\mathbf{x}(t)$,

$$\dot{\mathbf{x}}(t) = \mathbf{A}\mathbf{x}(t) + \mathbf{B}_{\phi}\mathbf{u}_{\phi}(t) + \mathbf{B}_{u}\mathbf{u}_{u}(t), \tag{14}$$

$$\mathbf{y}(t) = \mathbf{C}\mathbf{x}(t), \tag{15}$$

where $\mathbf{A}$ is the system matrix, $\mathbf{B}_u$ and $\mathbf{B}_\phi$ are the mechanical and electrical input matrices, $\mathbf{C}$ is the output matrix, $\mathbf{u}_u(t)$ and $\mathbf{u}_\phi(t)$ are the mechanical and electrical input vectors and $\mathbf{y}(t)$ is the output vector, given by

$$\mathbf{A} = \left[\begin{array}{cc} \mathbf{0} & \mathbf{I} \\ -\boldsymbol{\Omega} & -\boldsymbol{\Lambda} \end{array} \right], \tag{16}$$

$$\mathbf{B}_u = \left[\begin{array}{c} \mathbf{0} \\ \hat{\boldsymbol{\Psi}}^{\mathrm{T}} \end{array} \right], \mathbf{B}_\phi = \left[\begin{array}{c} \mathbf{0} \\ -\hat{\boldsymbol{\Psi}}^{\mathrm{T}}\mathbf{K}_{u\phi\mathrm{a}} \end{array} \right], \tag{17a,b}$$

$$\mathbf{C} = \left[\begin{array}{cc} avg\left\{-\mathbf{K}_{\phi\phi\mathrm{s}}^{-1}\mathbf{K}_{\phi u\mathrm{s}}\hat{\boldsymbol{\Psi}}\right\} & \mathbf{0} \\ \mathbf{0} & avg\left\{-\mathbf{K}_{\phi\phi\mathrm{s}}^{-1}\mathbf{K}_{\phi u\mathrm{s}}\hat{\boldsymbol{\Psi}}\right\} \end{array} \right], \tag{18}$$

$$\mathbf{u}_u(t) = \mathbf{F},\ \mathbf{u}_\phi(t) = \bar{\boldsymbol{\phi}}_{\mathrm{a}}(t), \tag{19a,b}$$

$$\mathbf{y}(t) = \left\{ \begin{array}{c} \bar{\boldsymbol{\phi}}_{\mathrm{s}}(t) \\ \dot{\bar{\boldsymbol{\phi}}}_{\mathrm{s}}(t) \end{array} \right\}. \tag{20}$$

In Equation (18) the notation $avg\{\cdot\}$ is utilized to denote that the signal induced by the piezoelectric sensors should be calculated from an average of the electrical DoF where an electrical FE separation of the electrodes was performed.

The open-loop system in Equations (14) and (15) consider two different input vectors, a mechanical disturbance force $\mathbf{u}_u(t)$ (primary excitation) and a control voltage $\mathbf{u}_\phi(t)$ (secondary excitation), and one output vector $\mathbf{y}(t)$ (sensor voltage and its derivative). In general we can consider that multiple inputs are applied to the smart beam (multiple forces and piezoelectric actuators) and that multiple outputs are obtained from multiple piezoelectric sensors.

3.2 Classical Control

With the purpose of reducing the vibrations we can establish a feedback loop where the signals produced by the piezoelectric sensors are amplified and fed back to the actuators in order to produce a secondary excitation that can cancel the primary force excitation. Therefore, the control voltage is given by

$$\mathbf{u}_\phi(t) = -\mathbf{G}\mathbf{y}(t), \tag{21}$$

where $\mathbf{G}$ is a feedback gain matrix defined according to the control law of interest. Substituting Equation (21) in (14), the closed-loop system is given by

$$\dot{\mathbf{x}}(t) = (\mathbf{A} - \mathbf{B}_\phi\mathbf{G}\mathbf{C})\,\mathbf{x}(t) + \mathbf{B}_u\mathbf{u}_u(t), \tag{22}$$

where the control vector $\mathbf{u}_\phi(t)$ is condensed in the state equations. From Equation (22) we can see that the gain matrix $\mathbf{G}$ controls the system through the modification of the closed-loop system poles. Therefore, if an adequate gain matrix and control law are established, the system vibration modes are attenuated through an increase in the modal damping ratio (the initial open-loop poles of matrix $\mathbf{A}$ are transformed into the highly damped ones of $\mathbf{A} - \mathbf{B}_\phi\mathbf{G}\mathbf{C}$). The gain selection and control system design of such feedback controllers can be done using either a pole-zero representation of the system (as in the root-locus method or pole placement, for example) or a frequency response representation (as, for example, in the Nyquist method). The stability is guaranteed provided the actuator and sensor are collocated [6]. Control systems where indirect methods are used for the definition of the feedback gains are often referred as *classical control*.

Assuming that a velocity feedback scheme is utilized, where the sensor output is differentiated, amplified, and then fed back into the actuator, the signal used in the velocity feedback is representative of the strain rate of the beam. Thus, a conventional term, *velocity feedback*, is used. In the velocity feedback two control algorithms are considered [12]. In the first one, which is termed *constant amplitude* velocity feedback (CAVF), the individual gain of the i-th piezoelectric actuator is defined according to the polarity of the i-th sensor voltage and, to denote that, the notation $sign(\cdot)$ is utilized. Hence, the feedback control voltage amplitude is constant, non-linear and

discontinuous, and the gain matrix is defined by

$$\mathbf{G} = \left[\begin{array}{cc} \mathbf{0} & diag\,(A_1, \ldots, A_i, \ldots, A_n)\; sign\,(\cdot) \end{array} \right], \tag{23}$$

where $diag\,(\cdot)$ denotes a diagonal matrix with the individual amplitudes A_i of the i-th control voltage, with $i = 1, \ldots, n$. Alternatively, a *constant gain* velocity feedback (CGVF) can be used, with the gain matrix defined by

$$\mathbf{G} = \left[\begin{array}{cc} \mathbf{0} & diag\,(G_1, \ldots, G_i, \ldots G_n) \end{array} \right], \tag{24}$$

where G_i is the individual gain of the i-th actuator. In this case the feedback control voltage is linear, continuous and decreases as the vibration velocity decays. It's worth to note that in Equation (22) the output matrix $\mathbf{C}$ assumes that all the sensor voltages and its derivatives are known for every sensor, but the zero matrices in Equations (23) and (24) indicate that only the voltage velocity is used in the feedback loop.

3.3 Optimal Control

In the previous section the values of the feedback gains were chosen to achieve some prescribed change in the dynamic properties of the system. However, the ultimate aim of the feedback control is often to reduce the motion of the mechanical system to the greatest possible extent and, in that case, the control system is said to act as a *regulator*. Systems where direct methods of designing feedback control systems which achieve the greatest possible reduction in the dynamic response are used are known as *optimal control* systems [5].

In optimal control the feedback control system is designed to minimize a cost function, or performance index, which is proportional to the required measure of the system's response and to the control inputs required to attenuate the response. The cost function can be chosen to be quadratically dependent on the output response and control input,

$$J = \int_0^{t_f} \left[\mathbf{y}^{\mathrm{T}}(t)\mathbf{Q}_y\mathbf{y}(t) + \mathbf{u}_\phi^{\mathrm{T}}(t)\mathbf{R}\mathbf{u}_\phi(t) \right] \mathrm{d}t + \mathbf{y}^{\mathrm{T}}(t_f)\mathbf{S}_y\mathbf{y}(t_f), \tag{25}$$

where $\mathbf{Q}_y$, $\mathbf{R}$ and $\mathbf{S}_y$ are the output, control input and terminal output condition positive-definite weighting matrices, respectively. Alternatively, the cost function J can also be written in another form,

$$J = \int_0^{t_f} \left[\mathbf{x}^{\mathrm{T}}(t)\mathbf{Q}_x\mathbf{x}(t) + \mathbf{u}_\phi^{\mathrm{T}}(t)\mathbf{R}\mathbf{u}_\phi(t) \right] \mathrm{d}t + \mathbf{x}^{\mathrm{T}}(t_f)\mathbf{S}_x\mathbf{x}(t_f), \tag{26}$$

in which $\mathbf{Q}_x$ and $\mathbf{S}_x$ are the state variable and terminal state condition positive semi-definite weighting matrices. Equation (26) is the form of cost function generally considered in optimal control. However, that all depends on the way the designer chooses to model the system, i.e., the way he suitable chooses the state variables and the system outputs.

As noted by Inman [3], modal control can be cast either in 'state space' form or 'physical space' form, i.e., in terms of the physical modes of the mechanical system. The present work considers an approach to control system design in which the state variables are chosen such that the unforced behavior of each state variable is relatively independent of the behavior of the other state variables, and the dynamics of the mechanical system is considered in terms of its modal response. Hence, one can choose as a performance index the cost function minimizing the outputs of the system (sensor voltage and its derivative), Equation (25), or, alternatively, one can chose to minimize the state variables (modal amplitudes), Equation (26). By a convenient definition of the state weighting matrix $\mathbf{Q}_x$, the modal gain matrix can be 'tuned' to give different design objectives. Assuming that all the modes (state variables) are observable and controllable, the cost function in Equation (26) provides independent control over the natural frequencies and damping ratios of each mode. That strategy is called *independent modal space control*, or IMSC [4]. Some convenient choices for the definition of the weighting matrices can be, for example,

$$\mathbf{R} = \begin{bmatrix} \mathbf{I} & \mathbf{0} \\ \mathbf{0} & \mathbf{I} \end{bmatrix}, \mathbf{Q}_y = \begin{bmatrix} \mathbf{I} & \mathbf{0} \\ \mathbf{0} & \mathbf{I} \end{bmatrix}, \mathbf{Q}_x = \begin{bmatrix} \mathbf{\Omega} & \mathbf{0} \\ \mathbf{0} & \mathbf{0} \end{bmatrix}, \tag{27a,b,c}$$

where a identity matrix $\mathbf{I}$ and diagonal matrix $\mathbf{\Omega}$ with the generic term ω_i^2 (squared natural frequency of the i-th mode) of size $(r \times r)$ are utilized.

It can be seen in reference [8] that the feedback control system which minimizes the cost function in Equation (26) for the linear time-invariant system defined in Equation (14), uses state feedback with a time-varying feedback gain matrix $\mathbf{K}_g^*(t)$, so that

$$\mathbf{u}_\phi(t) = -\mathbf{K}_g^*(t)\mathbf{x}(t). \tag{28}$$

The optimal time-varying feedback gain is given by $\mathbf{K}_g^* = \mathbf{R}^{-1}\mathbf{B}_\phi^{\mathrm{T}}\mathbf{P}(t)$, where $\mathbf{P}(t)$ is the solution of the *matrix Riccati equation*,

$$\dot{\mathbf{P}}(t) = -\mathbf{P}(t)\mathbf{A} - \mathbf{A}^{\mathrm{T}}\mathbf{P}(t) - \mathbf{Q}_x + \mathbf{P}(t)\mathbf{B}_\phi\mathbf{R}^{-1}\mathbf{B}_\phi^{\mathrm{T}}\mathbf{P}(t). \tag{29}$$

This control philosophy is called *linear quadratic regulator* (LQR). That regulator requires the knowledge of all the optimal gain values $\mathbf{K}_g^*(t)$ in the time interval $[0, t_f]$. However, the feedback gains of the LQR usually approach steady-state values far from the final time. Therefore, in applications where the control system is designed to operate for time periods that are long compared to the transient time of the optimal gains, it is reasonable to ignore the transient and use the steady-state gains, exclusively. The use of the steady-state LQR controller considerably simplifies the controller design and the analog and digital implementation. The steady-state feedback gain matrix is then given by

$$\mathbf{K}_g = \mathbf{R}^{-1}\mathbf{B}_\phi^{\mathrm{T}}\mathbf{P}^\infty, \tag{30}$$

in which $\mathbf{P}^\infty$ is the steady-state solution, $\lim_{t\longrightarrow\infty}\mathbf{P}(t)$, of the matrix Riccati equation. Therefore, considering a steady-state feedback gain $\mathbf{K}_g$ in Equation (28), the closed-loop state equations are given by

$$\dot{\mathbf{x}}(t) = \left(\mathbf{A} - \mathbf{B}_\phi\mathbf{K}_g\right)\mathbf{x}(t) + \mathbf{B}_u\mathbf{u}_u(t). \tag{31}$$

In the previous equations it was assumed that all the states were completely observable and therefore could be directly related to the outputs and used by the control system. However, that is not always the case and a more realistic approach would consider that where only the outputs $\mathbf{y}(t)$ can be known and measured. In order to be able to use the states information in the control system it will be necessary to estimate the states from a model of the system and a limited number of observations of the outputs. That estimation is made usually by a *state estimator* or *observer*. It is fed by the same known input signals as the mechanical system, $\mathbf{u}_\phi(t)$, and has its output $\hat{\mathbf{y}}(t)$ constantly compared with the output of the mechanical system, $\mathbf{y}(t)$. The objective is to ensure that the internal states of the electronic or digital state estimator, which can of course be directly measured, will track the internal states of the mechanical system, which can not be directly measured. The internal states of the state estimator are then used as estimates of the internal states of the mechanical system and fed back to the inputs to implement state variable feedback control.

However, the state variable estimates are very sensitive to any uncorrelated noise in the system, particularly measurement noise from the observed outputs of the mechanical system. Knowing the statistical properties of the various sources of noise in the mechanical system, and assuming white uncorrelated noise uniformly distributed in bandwidth, a 'optimal' state observer which minimizes the effects of plant and measurement noise is known as *Kalman filter*.

Considering the open-loop system in Equations (14) and (15) adjoined with plant and measurement noise, $\mathbf{w}(t)$ and $\mathbf{v}(t)$, yields

$$\dot{\mathbf{x}}(t) = \mathbf{A}\mathbf{x}(t) + \mathbf{B}_\phi \mathbf{u}_\phi(t) + \mathbf{B}_u \mathbf{u}_u(t) + \mathbf{B}_w \mathbf{w}(t), \tag{32}$$

$$\mathbf{y}(t) = \mathbf{C}\mathbf{x}(t) + \mathbf{v}(t). \tag{33}$$

where $\mathbf{B}_w$ is a plant noise input matrix. The plant and measurement noise are both assumed to be white, have a Gaussian probability density function and are assumed uncorrelated with the inputs. The correlation properties of the plant and measurement noise vectors are given by the correlation matrices

$$E\left[\mathbf{B}_w \mathbf{w}(t)\mathbf{w}^{\mathrm{T}}(t)\mathbf{B}_w^{\mathrm{T}}\right] = \mathbf{W},\ E\left[\mathbf{v}(t)\mathbf{v}^{\mathrm{T}}(t)\right] = \mathbf{V}, \tag{34a,b}$$

where E denotes the expectation operator. Considering a state estimator with the same dynamics as the system under control, which is assumed known, and the same known inputs, the estimator states $\hat{\mathbf{x}}$ would thus be governed by the equation

$$\dot{\hat{\mathbf{x}}}(t) = \mathbf{A}\hat{\mathbf{x}}(t) + \mathbf{B}_\phi \mathbf{u}_\phi(t) + \mathbf{K}_e^*(t)\left[\mathbf{C}\mathbf{x} + \mathbf{v}(t) - \mathbf{C}\hat{\mathbf{x}}(t)\right], \tag{35}$$

where $\hat{\mathbf{x}}(0) = 0$ and $\mathbf{K}_e^*(t)$ is known as the *Kalman gain matrix*. The last equation simulates the real system and penalizes the difference between the measured outputs, $\mathbf{C}\mathbf{x} + \mathbf{v}(t)$, and estimated outputs, $\mathbf{C}\hat{\mathbf{x}}(t)$. Defining the error between the true and estimated states as $\mathbf{e}(t) = \mathbf{x}(t) - \hat{\mathbf{x}}(t)$, the dynamic behavior of the Kalman filter can now be expressed as a coupled set of first order differential equations through the difference of Equations (32) and (35),

$$\dot{\mathbf{e}}(t) = \left[\mathbf{A} - \mathbf{K}_e^*(t)\mathbf{C}\right]\mathbf{e}(t) + \mathbf{B}_u \mathbf{u}_u(t) + \mathbf{B}_w \mathbf{w}(t) - \mathbf{K}_e^*(t)\mathbf{v}(t). \tag{36}$$

The Kalman gain matrix which leads to the optimal feedback controller is shown in reference [8] to be of the form $\mathbf{K}_e^*(t) = \mathbf{M}(t)\mathbf{C}^{\mathrm{T}}\mathbf{V}^{-1}$, where $\mathbf{M}(t)$ is the correlation matrix of the estimation error which is the solution of another Riccati equation,

$$\dot{\mathbf{M}}(t) = \mathbf{M}(t)\mathbf{A}^{\mathrm{T}} + \mathbf{A}\mathbf{M}(t) + \mathbf{W} - \mathbf{M}(t)\mathbf{C}^{\mathrm{T}}\mathbf{V}^{-1}\mathbf{C}\mathbf{M}(t), \tag{37}$$

which is usually solved with the initial condition $\mathbf{M}(0) = E[\mathbf{x}(0)\mathbf{x}^{\mathrm{T}}(0)]$. In a similar way to the steady-state LQR, the 'optimal' Kalman gain matrix $\mathbf{K}_e^*(t)$ in Equation (36) typically experiences a transient and then approaches steady-state as time increases from the initial time. In applications where the estimator is designed to operate for time periods that are long compared to the transient times of the Kalman gains, it is reasonable to ignore the transient and exclusively use the steady-state gains $\mathbf{K}_e$. This filter is suboptimal, but still yields excellent estimates in many cases. Additionally, the steady-state Kalman gain matrix is independent of the initial estimation error correlation matrix.

The equations for computing the Kalman gain have a striking resemblance to the equations for computing the LQR gain. In reference [8] the steady-state Kalman filter problem is shown to be equivalent to the steady-state LQR problem when appropriate substitutions are made. That correspondence is referred as *duality*. Hence, the duality relations between the steady-state Kalman filter and the steady state LQR allow to define the following correspondences: $\mathbf{A} \Leftrightarrow \mathbf{A}^{\mathrm{T}}$, $\mathbf{B} \Leftrightarrow \mathbf{C}^{\mathrm{T}}$, $\mathbf{K}_g \Leftrightarrow \mathbf{K}_e$, $\mathbf{Q} \Leftrightarrow \mathbf{W}$ and $\mathbf{R} \Leftrightarrow \mathbf{V}$ (note that the expressions on the right refer to the Kalman filter and the expressions on the left are for the LQR). Therefore, the LQR problem is mathematically equivalent to the Kalman filtering problem.

Combining the steady-state Kalman filter with the steady state LQR, the interrelated dynamic system will take take the form

$$\begin{Bmatrix} \dot{\mathbf{x}}(t) \\ \dot{\mathbf{e}}(t) \end{Bmatrix} = \begin{bmatrix} \mathbf{A} - \mathbf{B}_\phi\mathbf{K}_g & \mathbf{B}_\phi\mathbf{K}_g \\ \mathbf{0} & \mathbf{A} - \mathbf{K}_e\mathbf{C} \end{bmatrix} \begin{Bmatrix} \mathbf{x}(t) \\ \mathbf{e}(t) \end{Bmatrix} \tag{38}$$

$$+ \begin{bmatrix} \mathbf{B}_u \\ \mathbf{B}_u \end{bmatrix} \mathbf{u}_u(t) + \begin{bmatrix} \mathbf{B}_w & \mathbf{0} \\ \mathbf{B}_w & -\mathbf{K}_e \end{bmatrix} \begin{Bmatrix} \mathbf{w}(t) \\ \mathbf{v}(t) \end{Bmatrix}. \tag{39}$$

Because we must assume that the random perturbations (force disturbance and measurement noise) are Gaussian, this control philosophy is called *Linear Quadratic Gaussian* (LQG) control. The dynamics of the coupled controller and observer system is determined by the eigenvalues of the square system matrix in Equation (38). An important property of this system is known as the *deterministic separation principle*, in which the coupled system poles are exactly equal to those of the control system with perfect feedback control, given by the eigenvalues of $\mathbf{A} - \mathbf{B}_\phi\mathbf{K}_g$, and those of the observer alone, given by the eigenvalues of $\mathbf{A} - \mathbf{K}_e\mathbf{C}$. However, the closed-loop coupled system stability depends of the two sub-systems. The error will asymptotically be stable provided the observer poles have negative real components collocated, in the complex plan, as far as possible from the system poles so that the observer error reduces more rapidly than the system response.

4 Case Study

In this section the FE model is utilized in the evaluation of the classical and optimal active vibration control of a cantilever aluminum beam with two piezoelectric patches mounted in the surface (Figure 2). The displacement time history, for an initial displacement field and white noise force disturbance, and point receptance at the free end are evaluated with the open- and closed-loop systems.

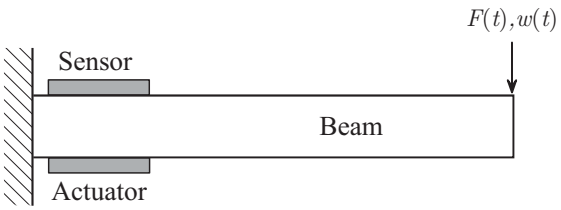

Figure 2: Cantilever smart piezoelectric beam.

The cantilever beam has 400 mm length, 2 mm thickness and 15 mm width, and the two piezoelectric patches (Philips Components – PLT $30/15/1$-PX5-N) have 30 mm length, 1 mm thickness and 15 mm width. The mechanical and electrical material properties of the aluminium beam and piezoelectric patches, PXE-5, are presented in Table 1. In the analysis a truncated modal model with the first four flexural modes was considered. The correspondent modal damping ratios were determined experimentally and their values are as follows: 1.71%, 0.72%, 0.42% and 0.41%. All the numerical calculations were performed in the MATLAB® environment.

Aluminium			
Young's modulus, E	70 GPa		
Poisson's ratio, ν	0.3		
Mass density, ρ	2710 Kg/m^3		
PXE-5			
Mat. coef., c_{11}^E	131.1 GPa	Piezo str. cst., d_{31}	-215×10^{-12} m/V
Mat. coef., c_{12}^E	7.984 GPa	Piezo str. cst., d_{33}	500×10^{-12} m/V
Mat. coef., c_{13}^E	8.439 GPa	Piezo str. cst., d_{15}	515×10^{-12} m/V
Mat. coef., c_{33}^E	12.31 GPa	Rel. str. perm., $\varepsilon_{11}^T/\varepsilon_0$	1800
Mat. coef., c_{44}^E	2.564 GPa	Rel. str. perm., $\varepsilon_{33}^T/\varepsilon_0$	2100
Mat. coef., c_{66}^E	2.564 GPa	Mass density, ρ	7800 Kg/m^3

Table 1: Material properties of the aluminium and PXE-5.

4.1 Initial Displacement Field

Consider an initial displacement field applied to the beam which induces a tip displacement of 1.5 mm. The tip displacement time history and control voltage for the CGVF and CAVF control systems are presented in Figure 3. The control gain $G = 0.4$ for the CGVF was chosen from a root locus analysis in order to increase the damping of the first mode as much as possible and, simultaneously, by a trial-and-error method in order to use control voltages within the desired range. According to the limit electric field strength of the piezoelectric patches (300 V/mm), the control voltage should be lower than 300 V. Exceeding that voltage may result in depolarization of the material so that the piezoelectric properties become less pronounced or disappear completely. For the CAVF, a constant amplitude $A = 250$ V was chosen and the control voltage was turned on at $t = 0$ s and turned off a $t = 0.2$ s. Furthermore, in the CAVF only the velocity polarity of the first-mode was considered in the feedback loop (perfect band-pass filter tuned to the first mode).

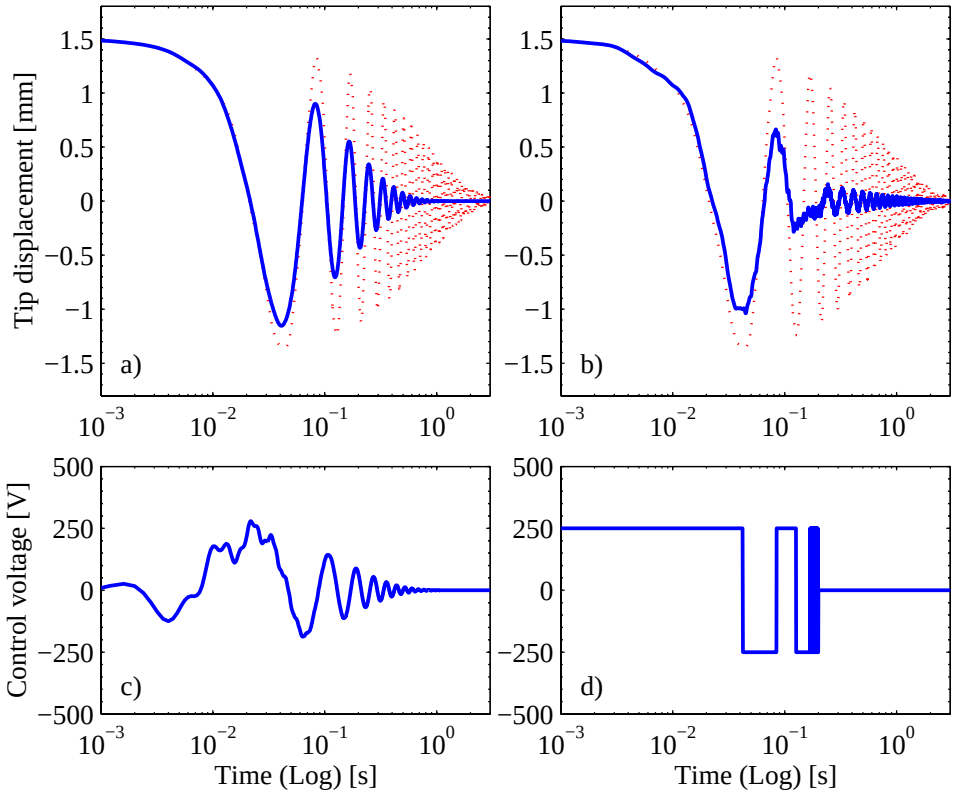

Figure 3: Tip displacement and control voltage for an initial displacement field with CGVF (a, c) and CAVF (b, d): ..... , open-loop; _____ , closed-loop.

As can be seen in Figure 3, the CGVF control manages to significantly attenuate the free tip displacement with an admissible control voltage. The closed-loop 5% settling time is equal to 0.5 s, which reveals a great improvement on the response

attenuation when compared with the open-loop one (2.3 s). Moreover, it presents a better performance than the CAVF (0.58 s). However, if we look at the 10% settling time, the CAVF control shows a faster attenuation capacity (0.24 s) than the CGVF (0.38 s).

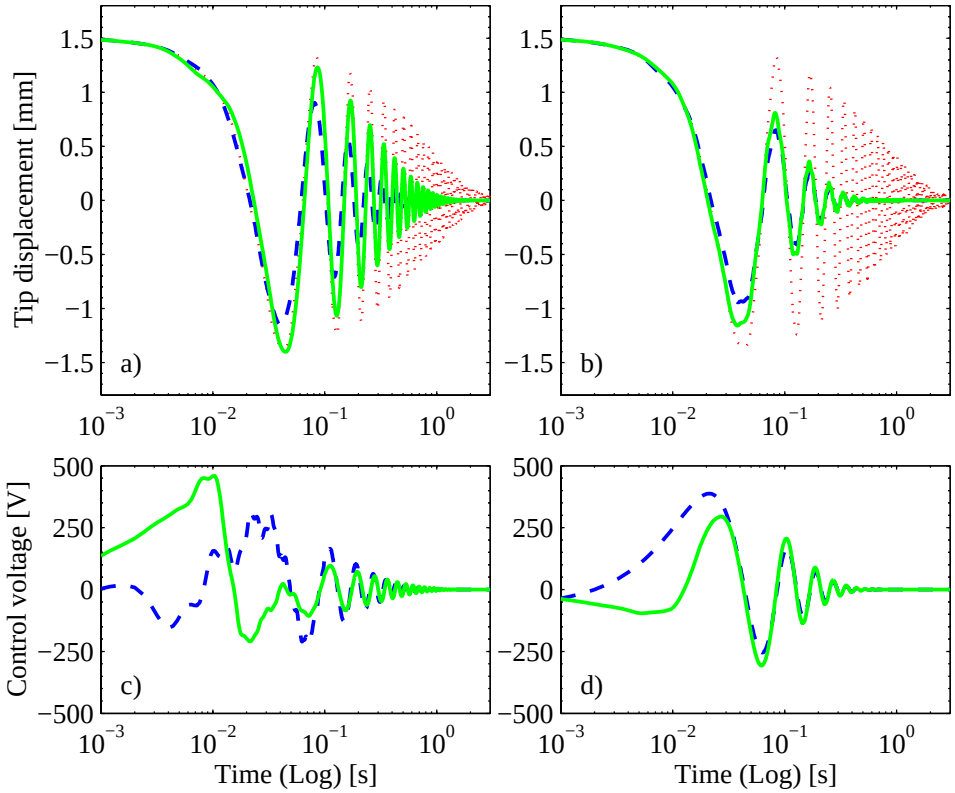

Figure 4: Tip displacement and control voltage for an initial displacement field with output $\mathbf{y}$ (a, c) and state $\mathbf{x}$ (b, d) weighting: ..... , open-loop; _ _ _ , closed-loop (LQR); ____ , closed-loop (LQG).

In Figure 4 the LQR and LQG controllers with output weighting (sensor voltage and its derivative) and state weighting (modal amplitudes and modal velocities) are utilized. It is assumed in the state estimation that only the sensor voltage, and not its derivative, is measured. That assumption corresponds to a more realistic approach and avoids the necessity of differentiating the sensor signal. For the output weighting case, the weighting matrices $\mathbf{Q}_y = diag\,(1,1)$ and $\mathbf{R} = 15$ were utilized, and for the state weighting case, the matrix $\mathbf{Q}_x = 1 \times 10^{10} diag\,(\omega_1^2, 0, \ldots, 0)$ was defined in order to mainly damp the first mode, and $\mathbf{R} = 30$ was chosen. For the LQG controller design, a white noise mechanical disturbance applied in the free end of the beam is modeled as plant noise. Therefore, in order to define the correlation matrix in Equation (34a) the equality $\mathbf{B}_w = \mathbf{B}_u$ should be considered. A plant noise vector (force disturbance) with $E[\mathbf{w}(t)\mathbf{w}^{\mathrm{T}}(t)] = 4 \times 10^{-4}$ N^2 and a sensor white noise disturbance with $E[\mathbf{v}(t)\mathbf{v}^{\mathrm{T}}(t)] = 1$ V^2 are considered for the definition of the noise

correlation matrices and Kalman gain design. However, the effects of the stochastic mechanical disturbance in the displacement time history will be considered only in the following sections. The results in Figures 4a and 4b show that the state estimator of the LQG controller with state weighting (only the first mode) has a better performance than the one with output weighting. Furthermore, in Figure 4a the displacements with the LQR and LQG have a significative difference in attenuation, with 5% settling times equal to 0.49 s and 0.89 s. Moreover, the LQR and LQG with state weighting in Figure 4b have the same 5% settling time (0.34 s), with the LQG requiring a lower control voltage, and when compared with the velocity feedback present a better performance.

4.2 White Noise Disturbance

As referred in the previous section, a white noise point force disturbance with variance equal to 4×10^{-4} N^2 is applied in the free end of the beam. The gains, amplitude and control parameters for all the control strategies are the same that were utilized in the previous section and only the output and state weighting matrices are changed to $\mathbf{R} = 1$ and $\mathbf{Q}_x = 1 \times 10^{10} diag\,(\omega_1^2, \omega_2^2, \omega_3^2, \omega_4^2, 0, \ldots, 0)$. This choice for the state weighting matrix is made in order to distribute the vibration control effort in bandwidth. However, the analysis is limited to the modal model bandwith (only the first four flexural modes are considered).

The open- and closed-loop tip displacements and control voltages for the white noise force disturbance evaluated with the CGVF and CAVF are presented in Figure 5. In Figure 6 the displacement and control voltages are evaluated with the LQR and LQG with output and state weighting. It can be seen that all the control systems manage to reduce the tip displacement significantly. When compared to the open-loop response standard deviation, which is equal to 0.57 mm, the closed-loop response standard deviations (with the respective control voltage standard deviations) for the CGVF and CAVF, 0.26 mm (79.6 V) and 0.20 mm (250 V), demonstrate the vibration control efficiency. Moreover, the LQR and LQG with output weighting present responses with standard deviations equal to 0.26 mm (97.4 V) and 0.28 mm (118 V), and the LQR and LQG with state weighting have their values equal to 0.16 mm (80 V) and 0.20 mm (72 V). The most effective control system is the LQR with state weighting. However, a state estimator is necessary, and the results achieved with the LQG (0.20 mm) are more realistic. Furthermore, they are equal to the ones obtained with the CAVF. However, if we look at the control voltages utilized, the most interesting one is the LQG with state weighting, with only 72 V, and the most inefficient, with the higher control voltage (250 V), is the CAVF.

4.3 Frequency Response Function

In order to analyse the capacity of the various control strategies on the frequency domain, the point receptances at the free end of the beam evaluated with the open- and closed-loop control systems are presented. With that purpose, the displacement time

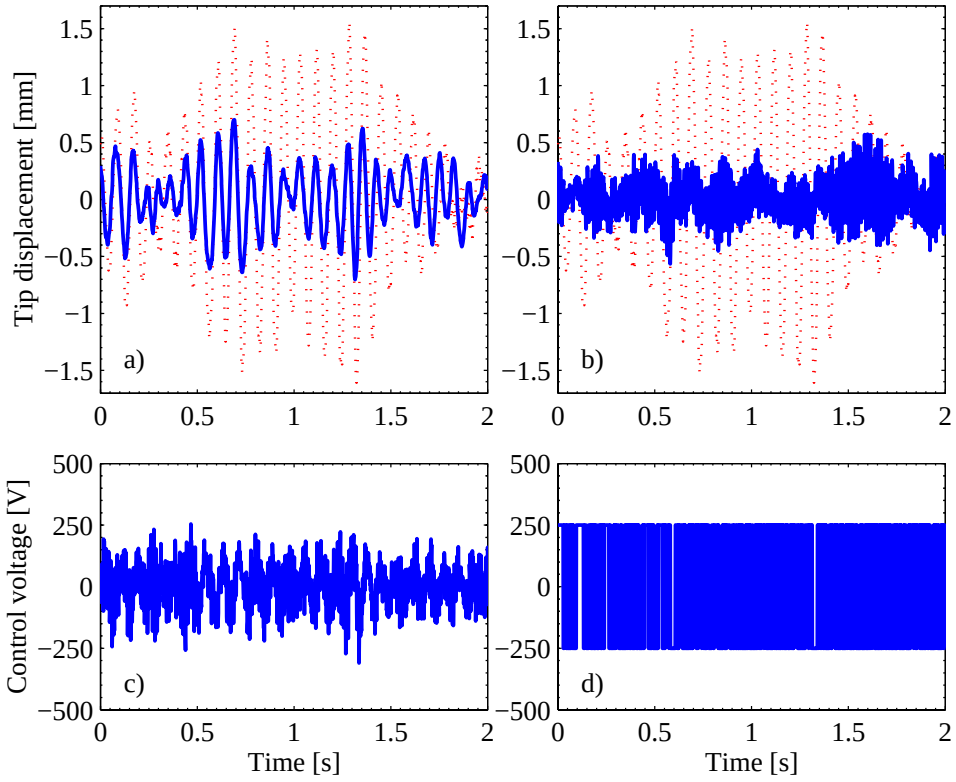

Figure 5: Tip displacement and control voltage for white noise point force disturbance with CGVF (a, c) and CAVF (b, d): ..... , open-loop; _____ , closed-loop.

histories for the white noise mechanical disturbance presented in the previous section are utilized to estimate the frequency response functions by a fast Fourier transform (FFT) computer algorithm. The open- and closed-loop point receptances for the CGVF and CAVF control are presented in Figure 7. The CAVF control significantly reduces the magnitude of the first resonance in approximately 27 dB, and increases the magnitudes of the other modes. In comparison, the CGAF doesn't manage to have such a good performance in the attenuation of the first mode, with a 8.6 dB reduction, but in compensation attenuation in all modes is achieved and the fourth mode is completely eliminated. Moreover, the natural frequencies are shifted.

In Figures 8 and 9 the point receptance for output $\mathbf{y}$ and state $\mathbf{x}$ weighting with the LQR and LQG controller are presented. The results show that the effects of the state estimation don't compromise the stability of the system, and that the output weighting LQG controller can have even a better performance than the LQR. A 8.8 dB and 9.4 dB attenuation of the first mode is achieved with the LQR and LQG controller with output weighting, respectively, and the resonant frequencies are shifted. If we now look at the results with state weighting (Figure 9), we can see that only the peak amplitudes are affected by the state estimator, and the natural frequencies remain the same. Furthermore, all the modes are damped, and a 12.2 dB and 10.7 dB reductions

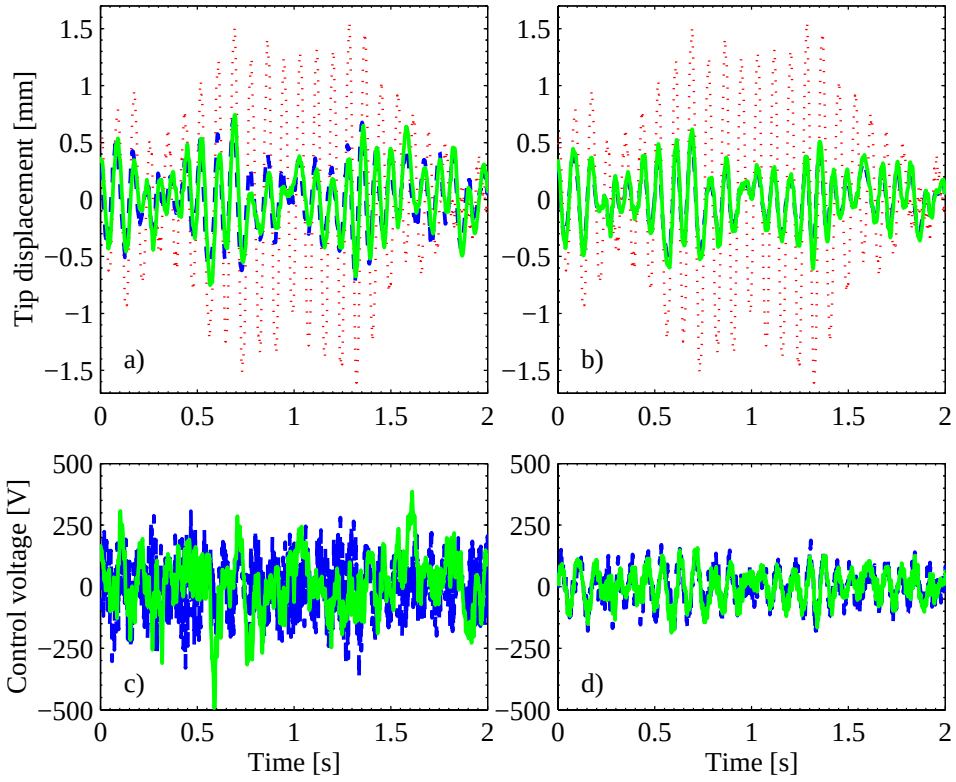

Figure 6: Tip displacement and control voltage for white noise point force disturbance with output $\mathbf{y}$ (a, c) and state $\mathbf{x}$ (b, d) weighting: ..... , open-loop; _ _ _ , closed-loop (LQR); ____ , closed-loop (LQG).

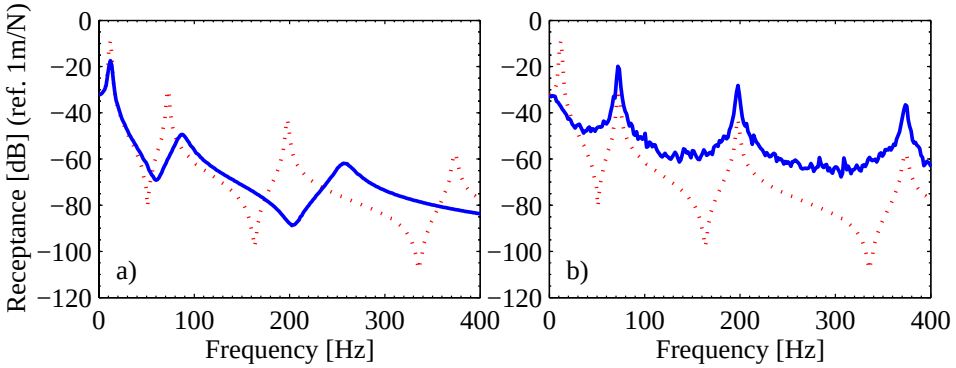

Figure 7: Point receptance with CGVF (a) and CAVF (b): ..... , open-loop; ____ , closed-loop.

of the first mode are achieved with the LQR and LQG controller with state weighting, respectively.

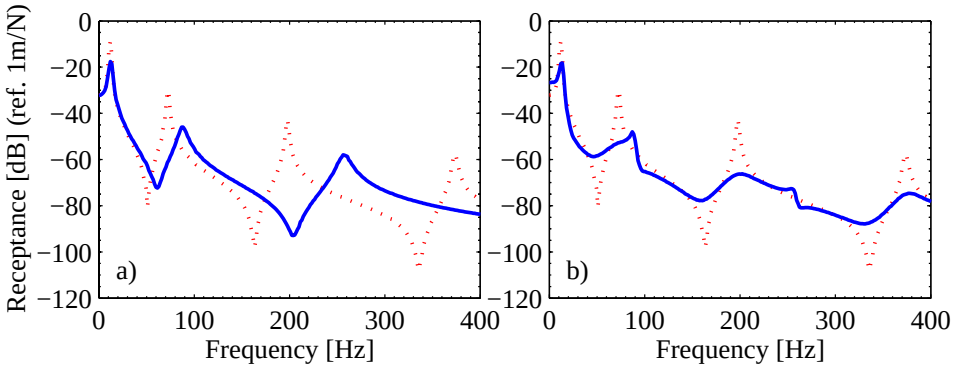

Figure 8: Point receptance with the LQR (a) and LQG (b) controller with output $\mathbf{y}$ weighting: ..... , open-loop; _____ , closed-loop.

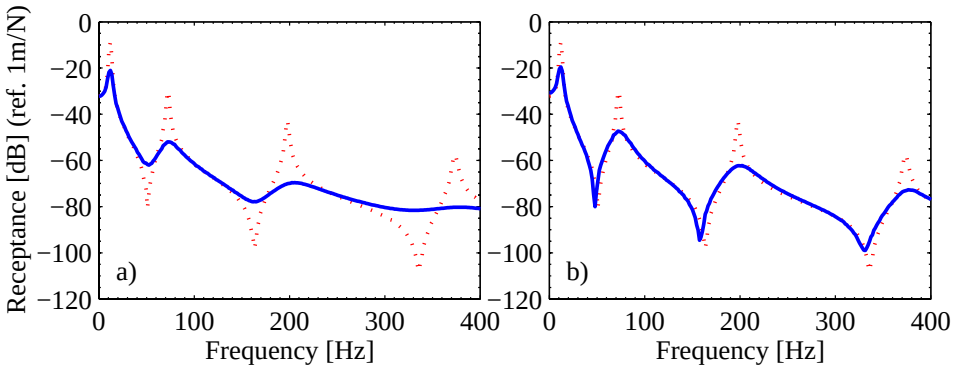

Figure 9: Point receptance with the LQR (a) and LQG (b) controller with state $\mathbf{x}$ weighting: ..... , open-loop; _____ , closed-loop.

5 Conclusion

The classical techniques can avoid the necessity of digital control reducing the time delays in the control system. However, the CGVF and CAVF strategies require the differentiation of the sensor voltage, which for noisy measurements can become troublesome. In compensation, stability is guaranteed provided the actuator and sensor are collocated. If one looks for adaptability in design, the optimal techniques, which require a model of the system, can be more interesting. The quantification of the control system's performance by a quadratic cost function provides the designer with lots of flexibility to perform trade-offs among various performance criteria. The relationship between cost function weights and performance criteria hold even for high-order and multiple input systems, where classical control becomes cumbersome. A major limitation of the LQR is that the entire state must be measured when generating the control. The LQG controller overcomes the need to measure the entire state by estimating the sate using a Kalman filter, which utilizes noisy partial output information, and some

modifications in its performance, which sometimes can improve the efficiency, often occur. However, observability and controllability spillover problems related with the reduced (truncated) model dynamics may compromise stability.

The case studies allow to compare the performances of the classical and optimal strategies. It was shown that for an initial displacement field the CAVF and LQG with the first mode weighted are the most interesting solutions. However, for a white noise disturbance, the CAVF only manages to reduce the mode under control, and the others are destabilized. Moreover, the LQG with all the modes weighted presents a better control in bandwidth with a lower control voltage. The output weighting LQG can also be an interesting strategy in situations where attenuation of the outputs is of interest. In the present analysis a resemblance in performance with the CGVF was shown.

References

[1] A. Benjeddou, *"Advances in Piezoelectric Finite Element Modeling of Adaptive Structural Elements"*, Computers and Structures, 76, 347-363, 2000.

[2] C.M.A Vasques, J. D. Rodrigues, *"Coupled Three-Layered Analysis of Smart Piezoelectric Beams with Different Electric Boundary Conditions"*, International Journal for Numerical Methods in Engineering, in revision.

[3] D.J. Inman, *"Vibration: With Control, Measurement, and Stability"*, Prentice Hall, Englewood Cliffs, New Jersey, USA, 1989.

[4] L. Meirovitch, *"Dynamics and Control of Structures"*, Wiley & Sons, New York, USA, 1990.

[5] C.R. Fuller, S.J. Elliott, P.A. Nelson, *"Active Control of Vibration"*, Academic Press, London, UK, 1996.

[6] A. Preumont, *"Vibration Control of Active Structures: An Introduction"*, Kluwer Academic Publishers, Dordrecht, NE, 1997.

[7] R. Alkhatib, M.F. Golnaraghi, *"Active Structural Vibration Control: A Review"*, The Shock and Vibration Digest, 35, 367-383, 2003.

[8] J.B. Burl, *"Linear Optimal Control: H_2 and H_∞ Methods"*, Addison-Wesley, Menlo Park, California, USA, 1999.

[9] M.J. Balas, *"Feedback Control of Flexible Systems"*, IEEE Transactions on Automatic Control, 23, 673-679, 1978.

[10] J.A. Waanders, *"Piezoelectric ceramics: Properties and applications"*, Philips Components, Eindhoven, NE, 1991.

[11] J.F. Nye, *"Physical Properties of Crystals: Their Representation by Tensors and Matrices"*, Clarendon Press, Oxford, UK, 1957.

[12] H.S. Tzou, *"Piezoelectric Shells: Distributed Sensing and Control of Continua"*, Kluwer Academic Publishers, Dordrecht, NE, 1993.